Structural and physical properties of mercury–iron selenide layers and quantum wells

D. Schikora, Th. Widmer, and K. Lischka
Universität/Gesamthochschule Paderborn, FB6-Physik, Warburger Strasse 100, D-33095 Paderborn, Germany

P. Schäfer, G. Machel, S. Luther, and M. von Ortenberg
Humboldt-Universität Berlin, Institut für Physik, Invalidenstraße 110, D-10115 Berlin, Germany
(Received 13 April 1995; revised manuscript received 12 June 1995)

Epitaxial layers and single quantum wells (SQW's) of Fermi-level pinned mercury–iron selenide (HgSe:Fe) have been grown by molecular-beam epitaxy on ZnTe buffer layers and characterized by *in situ* reflection high-energy electron-diffraction (RHEED) and high-field magnetospectroscopy investigations. The onset of strain relaxation at the critical thickness has been determined by time-dependent intensity-profile analysis of different reflexes in the RHEED pattern. In spite of the small mismatch and the very low growth temperature, a growth-mode transition from a two-dimensional–to–three-dimensional (2D-to-3D) Stranski-Krastanov growth mode has been identified, which coincides exactly with the critical thickness equilibrium value of about 61 nm predicted by the Matthews-Blakeslee theory. Due to this mechanism, the surface roughness transition region is extended and the onset of plastic relaxation is delayed up to a thickness of about 280 nm. Hall-effect measurements have been performed to determine the iron concentration in the HgSe layers below and above the Fermi-level pinning threshold concentration. With increasing iron concentration both a pronounced increase of the mobility and decrease of the Dingle temperature have been found in the layers. This agrees well with the present available data from HgSe:Fe bulk crystals and also with the values predicted by the short-range correlation model. However, the maximum carrier mobility of about 2.7×10^5 cm^{-3} measured in a 1.5-μm-thick HgSe:Fe layer indicates that long-range correlations also have to be considered in the transport mechanism of mercury–iron selenide. HgSe:Fe SQW's grown in the strained-layer region below the equilibrium critical thickness have been analyzed by Shubnikov–de Haas (SdH) measurements and Hall-effect measurements in magnetic fields up to 50 T. The existence of a two-dimensional electron system (Q2D) in the SQW has been confirmed by the cosine dependence of the SdH oscillation period. The subband splitting in the SQW in dependence of the quantum-well width has been investigated by Hall-resistance measurements. One subband has been identified experimentally in a 12-nm HgSe:Fe quantum well, whereas for high magnetic fields at least two subbands are measured in the 25-nm structures. The Landau-level splitting has been simulated using the Pidgeon-Brown model. In this way the subband splitting and the spin splitting observed experimentally can be explained. The broadening of the localized iron level has been determined from simulation curves.

I. INTRODUCTION

Mercury-iron selenide is a semimagnetic zero-gap semiconductor of the II-VI group, whose energy-band structure can be described by the inverted zinc-blende type. The statistical substitution of mercury by iron-ions generates a system of mixed valences $Fe^{2+/3+}$, energetically located about 210 meV above the conduction-band edge.[1] At a threshold Fe concentration of $n_{Fe}=5\times10^{18}$ cm^{-3}, the Fermi-energy of the system reaches the Fe donor level and becomes pinned to this energy. The Fermi-level pinned system shows a pronounced increase of the mobility and decrease of the Dingle temperature, due to spatial correlation effects of the $Fe^{2+/3+}$ system, suppressing the majority part of ionized impurity scattering. Whereas the experimentally observed reduction of the scattering rate is considered to be caused by spatial short-range correlation, the complete interaction mechanism is not yet clear.[2] The investigations of the physical and electronic properties of HgSe:Fe have been performed entirely on bulk crystals in the past. For dimension-reduced structures, some unusual electronic properties have been predicted:[3] In contrast to ordinary semiconductors, in the mixed-valence regime, modulation doping of Fe does not influence the Fermi energy and hence superlattices varying only in their scattering properties could be grown epitaxially. The externally controllable fluctuations of electrons between the delocalized conduction-band states and the localized states of iron should allow us to observe a three-dimensional analog of the quantum-hall effect (QHE) and to study the transition from this three-dimensional (3D) analog to the two-dimensional (2D) QHE. One can expect that the physical properties of dimension-reduced layer structures of mercury–iron selenide are influenced by elastic strain. The spin Hamiltonian parameters of iron should be sensitive to the ligand field, respectively, to the positions of the selenium atoms to which they are bound. Therefore, a careful investigation of strained-layer growth and lattice relaxation mechanism in mercury–iron selenide is a prerequisite to interpret the measurements and to compare it with the theoretical models. The influence of strain on the properties of mercury–iron selenide has not

0163-1829/95/52(16)/12072(9)/$06.00

been considered explicitly, neither in the experimental studies reported so far nor in the theoretical predictions. Successful epitaxial growth of pure HgSe has been reported by, Ref. 4, initiated by the technological requirement to find suited compounds as contact material in II-VI blue laser device structures. Investigations of the molecular-beam epitaxy (MBE) growth of mercury–iron selenide have not been carried out so far. Therefore, in this paper, we report about our experiments of the strained-layer growth of mercury–iron selenide on ZnTe buffer layers by MBE, in particular, the studies of the relaxation behavior at the critical thickness. We show the possibility of growing this semiconductor epitaxially with structural properties and transport properties, which are comparable to the best bulk crystals. Finally, we discuss magnetotransport measurements performed on single-quantum-well structures of Fermi-level pinned mercury–iron selenide, which were grown on ZnTe/GaAs substrates.

II. EXPERIMENTS

The experiments were carried out in a MBE system, which was designed and custom built according to the special requirements of the evaporation of Hg and the high-temperature thermal evaporation of Fe. The system was equipped with elemental solid sources of Se, Zn, and Te and a self-designed Hg-effusion cell of high capacity and flux stability. The beam-flux rates from the different evaporation cells were measured with an ion gauge beam-flux monitor. The Hg-to-Se flux ratio was varied between 50 and 100. The substrate temperature was routinely calibrated at the melting points of indium and lead. The GaAs (001) oriented substrates were heat cleaned and after deoxidization, immediately cooled down to the deposition temperature of 320 °C of the ZnTe buffer layer growth. After finishing the buffer layer growth, the HgSe:Fe layers were immediately grown on ZnTe at substrate temperatures between 70 °C and 120 °C. Both processes, the ZnTe buffer layer growth and the HgSe:Fe growth, were monitored by reflection high-energy electron diffraction (RHEED) using an electron gun operating at 15 keV. The RHEED pattern was recorded using a CCD camera and further analyzed with a commercial image-processing system. RHEED oscillation studies and RHEED intensity profile measurements have been performed. For high-resolution purposes the RHEED pattern was taken photographically from the RHEED screen and transferred to Photo-CD for further computer based analysis. The layer thickness measurements were carried out using mechanical step profilometer. The structural perfection of the epitaxial layers was investigated by high-resolution x-ray diffraction (HRXRD). The magnetotransport experiments were performed in dc fields up to 15 T using a superconducting solenoid and in pulsed fields up to 50 T using nondestructive coils. In both setups a phase-sensitive modulation technique[5] was applied for the actual measurements in a five-probe technique of the Hall-bar structured samples. The current of the order of some ten microamperes was chosen in such a way that Ohmic behavior of the samples was ensured.

III. PROPERTIES OF THE EPITAXIAL LAYERS

A. ZnTe buffer layers

It is well known from the epitaxial growth of heterostructures that mainly the structural quality of the substrate influences the structural perfection of the overgrown layer. ZnTe is one of the best adapted binary semiconductors to HgSe. The lattice mismatch between ZnTe and HgSe is about 0.3%. Furthermore, it has been demonstrated by several authors[6–9] that ZnTe can be grown successful on GaAs by MBE and metal-organic chemical-vapor deposition, although the lattice mismatch to GaAs is about 7.5%. The defect formation mechanism at the interface ZnTe-GaAs has been extensively investigated[6,7] by TEM. The lattice relaxation behavior and the surface reconstruction map have been determined by RHEED.[8] Because of the large mismatch of the ZnTe-GaAs system, the structural perfection of the ZnTe buffer layer depends strongly on the layer thickness. Therefore, it is important to determine, which layer thickness of the ZnTe buffer layer is sufficient for the subsequent growth of low-dimensional HgSe:Fe structures. It has been shown[10] from high-resolution x-ray measurements (HRXD) that reasonable half width [full width at half maximum] (FWHM) values of the rocking curve of 200 sec or less can be detected for layer thicknesses of more than 3 μm. The corresponding mosaic-block width l in the ZnTe layer, determined from these measurements, is of the order of $l \approx 80$ nm.[8] However, the penetration depth of the x-ray beams is about 2 μm for the (002) Bragg reflection and the measured mosaic-block parameters are an average over this depth range. Due to the strong varying mosaic size in very thin layers, HRXRD measurements are not suited to determine the mosaic parameters with sufficient accuracy. In order to be able to measure the mosaic-block width l of very thin epitaxial layers, a procedure was developed and tested,[11] which allows us to determine the mosaic-block width from the FWHM of selected RHEED streaks. The idea of this approach is to separate the contribution of the mosaic-block structured surface to the intensity distribution of the RHEED image from the contributions of the nonstationary surface roughness and from strain-induced streak broadening. This has been performed by numerical simulations of the intensity profile using a kinematic model. This model has been derived from an analog model of x-ray scattering in nonperfect crystals, which is described in detail in Ref. 12. In this simulation, a ZnTe (001) surface with known average mosaic-block tilt has been assumed. The dependence of the mosaic-block size from the FWHM of the RHEED streaks has been determined by a comparison of the calculated intensity profile and the intensity distribution measured by line scans during the growth of thick ZnTe layers. These layers were then analyzed by HRXRD to compare the results of both methods. The diffraction conditions for these RHEED experiments have been chosen in such a way that RHEED streak broadening, due to surface roughness and inhomogeneous surface strain, could be neglected.

Figure 1 shows the dependence of the mosaic-block

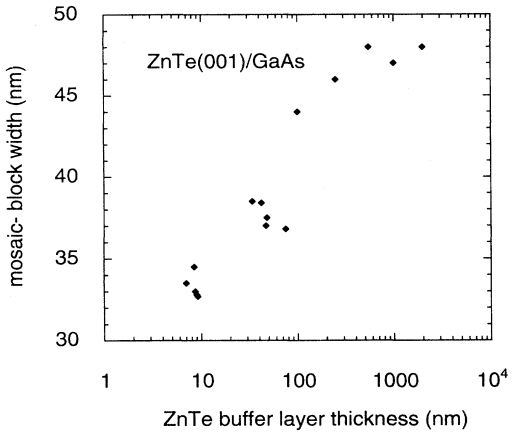

FIG. 1. Average mosaic-block size of a MBE grown ZnTe buffer layer in dependence of the layer thickness d determined from the FWHM of the (00) RHEED streak. The contribution of the mosaic-block structured surface to the broadening of the RHEED streak has been calculated by numerical simulations and measured experimentally by intensity line scans. It has been found that for thin ZnTe layers the mosaic-size saturates at $d > 0.4\,\mu$ m.

width of ZnTe from the layer thickness. It can be seen that the mosaic size in thin ZnTe layers measured by RHEED increases approximately linear to a layer thickness of about 0.4 μm and saturates gradually for layers thicker than 1.5 μm. This corresponds with an average mosaic-block width of about 45–50 nm and a mean mosaic tilting of about 100". These values complete the experimental data[8] of x-ray measurements. Therefore, we conclude that our procedure for determining the mosaic-block size during the growth from the FWHM of the RHEED streaks, can be applied, in particular, for thin epitaxial layers and represents a helpful supplement to x-ray measurements.

The ZnTe buffers layers used in this work were grown usually up to layer thicknesses of about 1.5–2.5 μm, which corresponds with mosaic-block widths of about 45–50 nm. It will be demonstrated in the following sections that these buffer layer parameters are reasonable for the subsequent growth of dimension reduced HgSe:Fe structures.

B. Measurements of the iron concentration

The determination of the chemical concentration of iron atoms in the HgSe lattice represents a key issue for the understanding of the transport measurements. However, there are some serious problems to determine the absolute iron concentration with sufficient accuracy. Due to the Fermi-level pinning at the threshold iron concentration of 5×10^{18} cm^{-3}, the Hall-effect carrier concentration above this value is independent of the iron concentration and cannot be taken as a measure. Furthermore, a direct determination of the iron flux density in the MBE cannot be performed, because of the high mercury background pressure in the growth chamber. The aspired concentration range of about $n_{Fe}=1\times10^{19}$ cm^{-3} restricts the possibility to use secondary-ion mass spectrometry. On the other hand, there are some simplifications resulting from the growth process itself. The substrate temperature for the growth of HgSe on ZnTe is in the order of 70 °C–120 °C. Because of this unusual low growth temperatures, one can assume a sticking probability for the incoming iron atoms of about one. We did not find any evidence that the thermal evaporation of iron generates significant lattice or surface damage during the growth. Therefore, the background carrier concentration of pure HgSe is not influenced by the iron doping and can be taken as a constant. If we assume further that each condensed iron atom raises the total carrier number in the conduction band by one, the iron concentration results as the difference between the carrier concentration of mercury–iron selenide and the background carrier concentration of pure HgSe. On these preconditions, one can determine the evaporation-temperature dependence of the iron concentration by Hall-effect measurements below the Fermi-level pinning threshold.

The dependence found between the evaporation temperature of the iron effusion cell and the resulting iron concentration in the layer can be described exactly by a Hertz-Knudsen formalism. Therefore, the Hall-effect carrier-concentration data from low-level-doped samples can be used for calibration purposes.[17] To be able to extrapolate this dependence to the actual interesting range above the Fermi-level pinning threshold, an additional assumption has to be made. During the epitaxial growth of Fermi-level pinned systems, electrostatic screening effects have been observed,[13] influenced the sticking coefficients of the doping species and consequently the resulting carrier concentration. We could not measure such effects, therefore an independence of the iron sticking coefficient from the amount of iron condensed in the surface lattice has to be assumed. The Fe-concentration values determined for our heavily doped HgSe:Fe layers agree with the Hall mobility versus iron concentration curve, as known from bulk crystal measurements[15,16] and from theoretical predictions.[14] We observe a decrease in the Hall mobility with increasing iron concentration below the pinning level and a strong increase of the Hall mobility, due to the spatial correlation of the Fe^{3+} states above the pinning threshold. We have found that the mobility in epitaxial HgSe:Fe layers, which were grown usually up to 1 μm thickness, are at least comparable with the largest values measured in bulk crystals. The maximum mobility of about 2.7×10^5 cm^2/V s has been measured[17] in a 1.5-μm-thick HgSe:Fe layer. This is significantly larger than the theoretical mobility values reported so far.[14–16] However, this calculation has been performed assuming a short-rang-correlation model (SCR). Similar deviations from the SCR model to higher mobility values are also found by Monte Carlo simulations (MC) of the iron-concentration dependent electron mobility.[32] In this MC study, the higher mobility values are attributed to long-

range correlations in contrast to the SCR model, which completely neglects such effects. Therefore, our results confirm experimentally that at least second-nearest-neighbor correlations have to be considered in the theoretical models about the transport mechanism in mercury–iron selenide. The quantitative analysis of the Dingle temperature in MBE HgSe:Fe layers and bulk crystals, which has been performed in detail in Ref. 17, yields an average value of $T_{\text{Dingle}}=8.25$ K for the MBE layers and $T_{\text{Dingle}}=10.5$ K for the bulk crystals compared. This result also proves that the structural perfection and consequently the electronic properties of the MBE grown HgSe:Fe layers are comparable with the best bulk crystal data and, therefore, meet the preconditions for the growth of dimension-reduced structures.

IV. CRITICAL THICKNESS DETERMINATION

Due to the low lattice mismatch between HgSe ($a_0=0.6084$ nm) and ZnTe ($a_0=0.6102$ nm), it is impossible to detect the critical layer thickness for HgSe by *in situ* analysis of the RHEED streak spacing. The resolution R of a RHEED lattice-constants measurement taken directly from a normal phosphorous RHEED screen is in the best case in the order of $R=\Delta a/a\sim 10^2$, where a is the lattice constant being measured and Δa is its change produced by plastic deformation of the layer at the critical thickness. Since misfit less than R cannot be resolved, one has to use for HgSe/ZnTe ($\Delta a/a=3\times 10^{-3}$) either *ex situ* methods, in particular, x-ray measurements, or to change the detection principle for the scattered electrons in the RHEED system. Figure 2 shows x-ray measurements that have been carried out to determine a critical layer thickness of HgSe:Fe on ZnTe. It can be seen that the half width (FWHM) of the HgSe:Fe rocking curve (marked by squares) exhibits a minimum at a layer thickness of approximately 0.2 μm. At this layer thickness, the FWHM increases abruptly reaching a maximum at about 0.4-μm layer thickness. From this curve, one can derive a preliminary critical thickness value $h_{c1}^{\text{obs}}=0.2$ μm, which is much larger than the equilibrium value resulting from the Matthews-Blakesleee model[19] $h_c^{\text{MB}}=61$ nm. We attribute this difference mainly to the limited resolution of the x-ray rocking curve analysis, because this method is able to detect the generation of dislocations, due to strain relaxation only when a certain threshold of misfit-dislocation density has been exceeded. This explains the difference between our measurement and the equilibrium value predicted by the critical thickness theories,[18–20] in particular, to the most accepted Matthews-Blakeslee model.[19] This theory represents the balance point of elastic and plastic deformation and, consequently, the lowest limit of the critical layer thickness. It is commonly accepted that measurements closer to the equilibrium value of the critical thickness require experimental methods, which are able to detect very low densities of misfit dislocations or very low amounts of strain.[21] Besides the rocking-curve measurements, we have used the x-ray bond method for the determination of the relaxation in the HgSe:Fe lattice by precision lattice-constant measurements. By this method, reliable data could be measured up to a minimum layer thickness of about 200 nm. These results are also shown in Fig. 2 marked by circles. At a layer thickness of about 200 nm, the HgSe:Fe lattice is still fully strained and exhibits as well the lattice constant as the rocking curve half width of the ZnTe buffer layer. At a layer thickness of 300 nm the HgSe is already relaxed at 43% to its own bulk lattice-constant value. These bond measurements confirm completely the rocking-curve data shown in Fig. 2. To get further information on the lattice relaxation process and its dynamical behavior in HgSe:Fe, we have performed a time-dependent intensity-profile analysis of different reflexes in the RHEED pattern. Similar investigations have been successfully carried out for epitaxial systems with large lattice mismatch like $In_xGa_{1-x}As/GaAs$,[22–24] SiGe/Si,[25,26] or EuTe/PbTe,[27] where a growth mode transition occurs at the critical thickness. Due to the influence of the strain field on the planar layer-by-layer growing surface, the surface roughness changes abruptly near the balance point of maximum elastic deformation and minimum plastic relaxation. It has been shown[28] theoretically that a nominally flat growing surface, which is elastically stressed, becomes unstable and tends to form 3D islands. To identify this transition from the van der Merwe growth mode to the Stranski-Krastanov growth mode, as well RHEED oscillations, measurements[22–24] as Kikuchi-line intensity measurements[27] have been reported. According to this investigation, a model has been proposed[24] that a strain-induced growth-mode transition should be observable only for systems with a mismatch of at least 2%. The HgSe:Fe/ZnTe system, which is in contrast to that of low mismatch, has not been investigated to its strain relaxation behavior so far. One should ex-

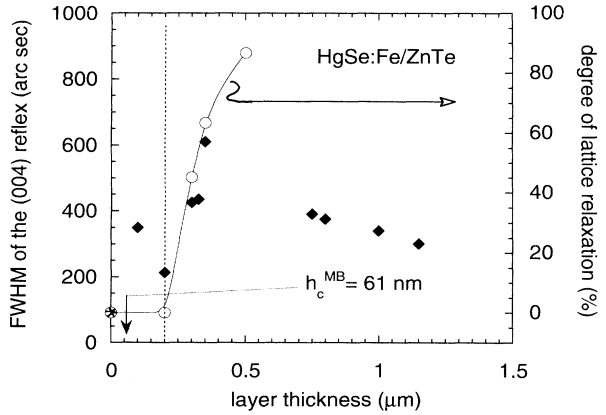

FIG. 2. FWHM of the x-ray rocking curve (black squares) and lattice relaxation degree (circles) of HgSe:Fe versus layer thickness. The minimum of the FWHM at 0.2 μm reflects a critical thickness detected here within the limits of the x-ray-diffraction method. Therefore, we have called it "observed critical thickness" h_c^{obs}, which is by a factor of about four larger, than the equilibrium value predicted by the Matthews-Blakeslee model. The relaxation degree measured by the x-ray bond-method confirms that at 0.2 μm the HgSe:Fe layer is still completely strained.

pect at the first glance that no change of the growth mode can take place, because this requires besides sufficient strain energy, as driving force, also a high adatom mobility to rearrange the flat growing HgSe:Fe surface. Both would be surprising for our very low growth temperatures of about 70 °C–120 °C. Additionally the enormous excess of Hg during the growth of HgSe:Fe lowers the free-surface energy and acts as a kind of surfactant stabilizing the 2D growth mode. Figure 3 shows the FWHM of the (00) RHEED streak, measured in the direction perpendicular to the shadow edge in dependence of the HgSe:Fe layer thickness. Immediately after the beginning of the growth of HgSe on ZnTe, we observe a high FWHM value, indicating the predominant Stranski-Krastanov character during the initial heterogeneous nucleation. Furthermore, it can be seen from Fig. 3 that the RHEED reflect half width drops down very quickly after finishing the initial stage and remains constant up to a layer thickness of about ≈ 60 nm. Then the FWHM increases abruptly and remains again constant up to a layer thickness of about ≈ 280 nm. At this point, a continuous decreases of the FWHM can be observed. This value of 280 nm is obviously associated with the minimum of the x-ray rocking-curve half width discussed in Fig. 2 at about 200 nm and the significant lattice relaxation degree of about 63% detected by the x-ray bond method at about 300 nm. We know from these x-ray measurements that at least the main part of the plastic relaxation must occur between 200 and 300 nm thickness. The value of 280 nm found by RHEED-FWHM measurements confirms this and indicates more precisely the beginning of this process. Therefore, the steplike changes in the RHEED-FWHM curve below 280 nm must be caused by other effects and cannot be attributed to the plastic relaxation itself. To identify this, very special diffraction conditions in the RHEED experiments have been chosen. We select a glance angle and a acceleration voltage which satisfies the out-phase condition for a layer-by-layer growing HgSe:Fe surface. However, this selected glance angle fulfills also the in-phase condition exactly, if the surface consists of growth islands of two monolayers height. During the growth experiment, the RHEED-FWHM is sensitive to the surface roughness as long as the growth takes place in the 2D growth mode and becomes insensitive to the surface roughness, if the system executes a growth mode transition. On the basis of this diffraction conditions, the curve in Fig. 3. can be discussed. After the short nucleation-related change at the beginning of growth, the FWHM remains constant up to a layer thickness of about 60 nm, reflecting a stable layer-by-layer growth mode. At this thickness, which coincides exactly with the critical layer thickness according to the Matthews-Blakeslee model, the surface roughness changes significantly, which is indicated by the abrupt increase of the FWHM. After this transition, the FWHM again remains constant up to the layer thickness of about 280 nm. We explain this constant FWHM maximum over a wide thickness range with a change in the diffraction parameters from the out-phase to the in-phase condition, which is insensitive to the surface roughness. This insensitivity again is connected with the existence of a growth islands of about two monolayers in height. Therefore, we attribute the characteristic shape of the FWHM versus thickness curve to a growth-mode transition from a 2D van der Merwe growth to a 3D growth mode. This transition occurs close to $h_c^{eq}=h_c^{MB}=61$ nm, because of the maximum strain energy in the HgSe layer at this thickness. Then the system changes the roughness of the growing surface, because a regularly corrugated surface morphology consisting of 3D islands of multiatomic height is energetically favorable in comparison to a flat surface. The additional cost of free-surface energy is overcompensated by the energy gained from the elastic deformation of the 3D islands. This 3D growth mode is stable between 60–280 nm and obviously delays the onset of the plastic relaxation of the HgSe:Fe lattice. At 280-nm layer thickness, the plastic deformation occurs by formation of misfit dislocations. The introduction of misfit dislocations at this thickness is accompanied by a decreasing RHEED half width in Fig. 3, because the flat surface is again energetically favored, due to the reduced strain energy, and the system switches back to a stable 2D layer-by-layer growth mode. The layer thickness dependence of the lattice relaxation degree, which has been determined by bond measurements, confirms the interpretation of the dynamical behavior of the strain relaxation, which has been found by time-dependent intensity-profile analysis of the RHEED (00) streak.

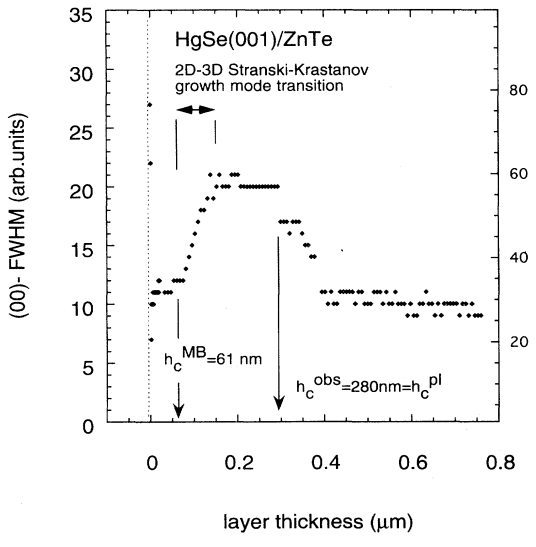

FIG. 3. FWHM of the (00) streak of the HgSe:Fe RHEED pattern versus layer thickness. The curve exhibits two plateaus of constant FWHM between 1–60 nm and between 100–280 nm. The abrupt increase of the FWHM, due to surface roughening, coincides with the equilibrium value of the critical thickness of 61 nm and reflects the transition of the two-dimensional layer growth to the three-dimensional Stranski-Krastanov mode. The second plateau corresponds with the stability of strained three-dimensional islands on the growing surface, which abruptly changes at 280 nm, reflecting the onset of the plastic deformation at h_c^{pl}.

From this investigation, we conclude that the surface mobility of the adatoms in our growth process is high enough to rebuild the surface. The extended range of metastability regarding to the plastic deformation between 60 and 280 nm may be attributed to the very low growth temperature in our MBE experiments.

V. MAGNETOTRANSPORT INVESTIGATIONS

Single-quantum wells (SQW) of HgSe:Fe on ZnTe substrates have been grown for measurements of the Hall-effect and Shubnikov–de Haas effect. The quantum wells were grown in the strained-layer region below the critical thickness of 61 nm. The layer thickness has been varied between 12 and 50 nm. The SQW were grown directly on ZnTe(001) buffer layers. The iron concentration was about 4×10^{19} cm^{-3}. To corroborate the existence of a Q2D system in the HgSe:Fe, the angular dependence of the transverse magnetoresistance has been measured for the magnetic-field range $0<B<15$ T and for the angle θ between the surface and the magnetic-field direction in the range $0\leq\theta\leq60°$. Figure 4 shows the changing of the position of the 9th Landau level $l=9$ (marked by arrows) with the orientation of the magnetic field. The characteristic features of the SdH traces shift towards to higher total field values, due to the decreasing perpendicular field component B. For ideal 2D systems, the SdH oscillation period $\Delta_i(1/B)$ ($i=$ subband index) and the reciprocal fundamental magnetic fields $1/B_{\rm fi}$ are proportional to $\cos\theta$,[29]

$$2e(\cos\theta)/h\,\Delta_i(1/B)=2eB_{\rm fi}(\cos\theta)/h\ . \qquad (1)$$

The $\cos\theta$ dependence of the oscillation shift in tilted fields as demonstrated in Fig. 5 for the Landau level $1=9$ proves the existence of a Q2D system in the HgSe:Fe single-quantum well of 25 nm thickness The evaluation of the SdH period for $\theta=0$ results in a carrier concentration of 4.1×10^{18} cm^3. The slight decrease of this value in comparison with the pinning concentration of about $n=5.0\times10^{18}$ cm^{-3} indicates that the effective subband is only slightly elevated above the band edge. It should be noted that no significant fine structure in the SdH oscillations of HgSe:Fe SQW could be detected up to 15 T. Using pulsed magnetic fields, the measurements were extended up to 50 T. In Fig. 6, the data for both the transverse magnetoresistance and the Hall effect for the same sample are extended to higher fields and now clearly exhibit the interference pattern of the SdH oscillations of two different subbands. Using standard evaluation techniques, the different oscillations could be associated with the two subbands denoted as a and b in Fig. 6. There is the indication of at least one more subband close to the Fermi energy by the slowly oscillating envelope. The assignment of the oscillation peaks is qualitatively confirmed by a model calculation of the two Landau ladders in the SQW. Despite the fact that the SQW has asymmetric interfaces at the confinement (vacuum and ZnTe), the potential shape is well approximated by a symmetric square-well potential, due to the short screening length in the high-concentration carrier system. In a crude approximation, the subband energies in this model potentials were calculated taking into account the energy dependence of the effective mass, resulting in an energy splitting of the subbands of about 30 meV. The usual Landau ladders calculated in the Pidgeon-Brown model for $k_z=0$ were superimposed on the subband energies. As a matter of fact, this means that any coupling of the motion perpendicular and parallel to the magnetic field is neglected. Nevertheless the results of this model support the understanding of the presented data. The data of the Hall resistance exhibit a structure corresponding to the SdH oscillations and indicate the gradual manifestation

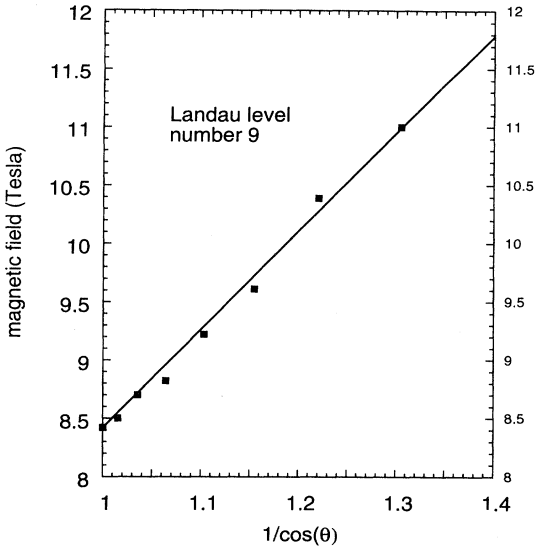

FIG. 5. Cosine dependence of the shift of the ninth Landau level in tilted magnetic fields. The dependence corroborates the existence of a Q2D system in the single-quantum well.

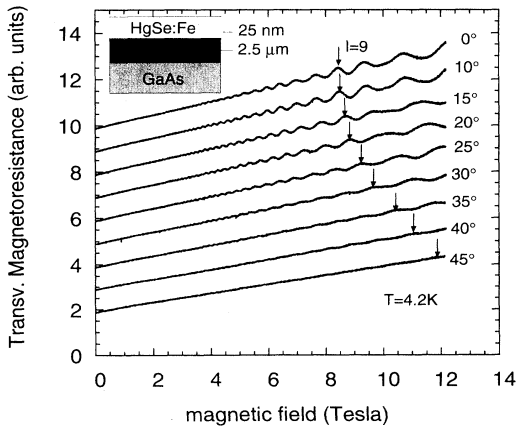

FIG. 4. Transversal magnetoresistance of a 25-nm HgSe:Fe single-quantum-well grown on ZnTe. The ninth Landau-level $I=9$ (marked by arrows) shifts in tilted magnetic fields.

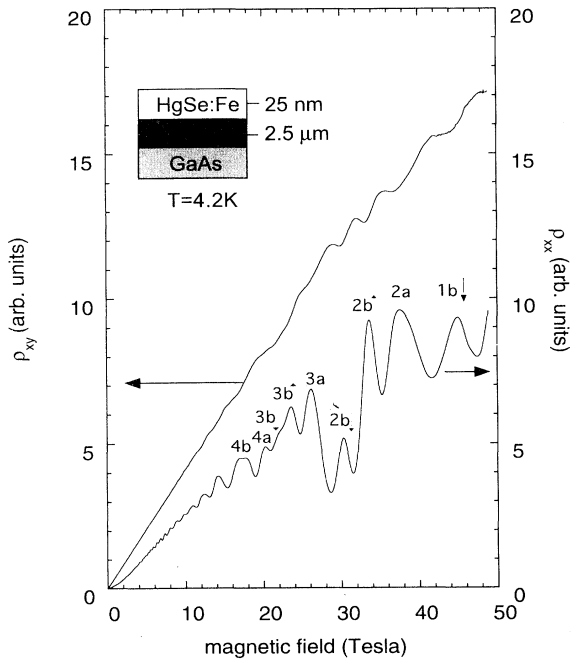

FIG. 6. Hall resistance and transversal magnetoresistance versus magnetic field of a 25-nm HgSe:Fe SQW. At least two different subbands are resolvable. The maximum values in the transversal magnetoresistance, which could be attributed to different subbands in the quantum well, are denoted by *a* and *b*. The assignment of the SdH maxima to the Landau levels have been performed using a simulation of the Landau-level splitting, which is described in Ref. 33.

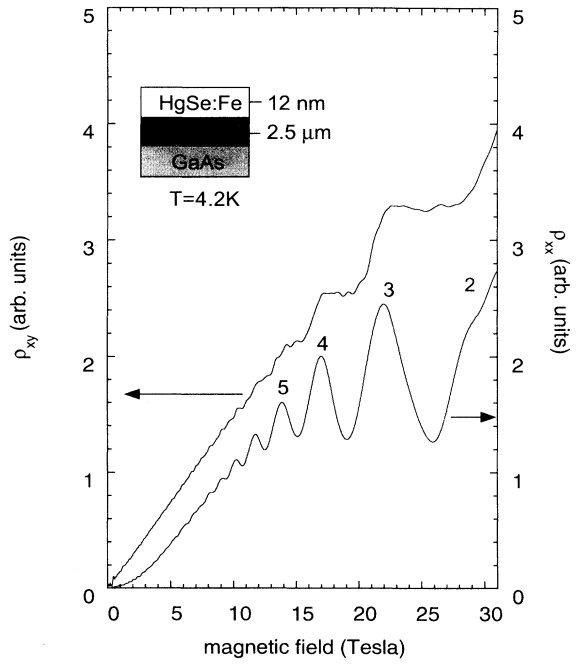

FIG. 7. Hall resistance and transversal magnetoresistance versus magnetic field for a 12-nm HgSe:Fe SQW. The Landau quantum number *l* is indicated and makes clear that the system is near the quantum limit. The data exhibit clearly one Q2D Landau ladder without spin splitting of a highly degenerated carrier system corresponding to bulk concentration $n=3.8\times10^{18}$ cm^{-3}.

quantum-Hall-effect-like plateaus. The actual mechanism leading to the plateau structure may be different for HgSe:Fe compared to other materials,[30] since in HgSe:Fe carrier fluctuations between the localized iron level and the quasifree states play a dominant role.

In contrast to the 25-nm SQW, the data of a quantum well having only 12-nm width indicate only one occupied subband, as shown in Fig. 7. This figure illustrates the typical behavior of a two-dimensional electron system (Q2D) in an external magnetic field. The Hall resistance increases linearly with the magnetic field and exhibits quantum-Hall plateaus, which are located according to $\rho_{xy}=h/le^2$. Here, ρ_{xy} is the Hall resistance, h is Planck's constant, e is the elementary charge, and 1 the Landau-level number. The transversal magnetoresistance is periodically reduced whenever the Fermi level lies between two Landau levels. Because of the strong degeneracy of the electron system in heavily doped HgSe:Fe, these effects can be observed only in high magnetic field with $B>20$ T. The data exhibit clearly one Q2D Landau ladder without spin splitting of a highly degenerated carrier system corresponding to a bulk concentration $n=3.8\times10^{18}$ cm^{-3}. This means that the lowest subband has been considerably elevated with respect to the 25-nm SQW, due to the additional confinement. The Landau quantum number 1 is indicated and makes clear that the system is near the quantum limit. Supposing the carrier fluctuation model as the dominant mechanism for the manifestation of the plateaus in the Hall resistance, additional useful information with regard to the localized density of states of the Fe^{2+} ions can be obtained.[30] Because the density of states $D_{Fe2+}(E)$ of the Fe^{2+} ions is finite, the Fermi energy is not complete constant, but oscillates with an amplitude depending on both the slope and the absolute value of $D_{Fe2+}(E)$. This results in a more gradual transition from one plateau to the next in the Q2D limit of the quantum-Hall effect. This characteristic behavior has been simulated[30] using a Lorentz-like broadening of the Fe^{2+} level,

$$D_{Fe2+}(E)+\{(\Gamma/\pi)/[(E-E_0)^2+\Gamma^2]\}n\mathrm{Fe}^{2+} . \quad (2)$$

The parameter E_0 has been chosen in such a way that the Fermi energy for zero magnetic field is the same for all the different values of the damping parameter Γ. Figure 8 shows the dependence of the plateau-width ratio (PWR) from the damping parameter Γ in HgSe:Fe for $n_{Fe}^{2+}=5\times10^{19}$ cm^{-3}.[30] The plateau-width ratio (PWR) correlates the width of the lth plateau at $\Gamma>0$ with the plateau width for $\Gamma=0$. A PWR value of 0.5 is estimated for the 12-nm SQW shown in Fig. 7. As it is indicated in Fig. 8, this value corresponds to a Γ value of about 5.8

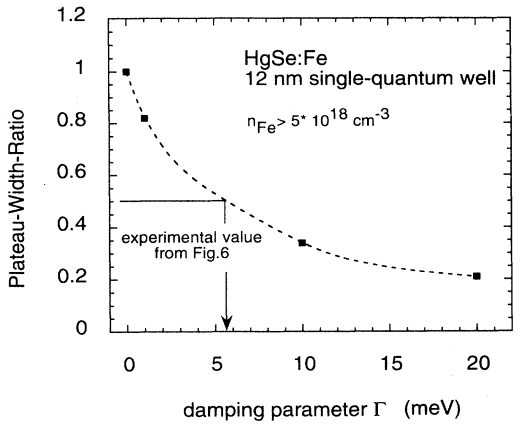

FIG. 8. Plateau-width ratio (PWR) versus damping parameter Γ for HgSe:Fe derived from a simulated curve of the two-dimensional quantum-Hall effect (Ref. 30). The measured plateau-width ratio for a 12-m HgSe:Fe SQW of about 0.5 corresponds to a damping parameter value of about 5.8 +/− 0.6 meV.

meV +/−0.6 meV, which is in agreement with values reported so far.[31] Because the slope of the transition range between the plateaus is directly related to the value of $D_{Fe2+}(E)$, we conclude from this investigations that a damping parameter Γ in the order of 6 meV or smaller should allow us to observe experimentally in further studies the predicted[3] gradual transition from the two-dimensional quantum-Hall effect to the three-dimensional analog of the QHE. Besides this, the structural and physical properties of our MBE grown mercury–iron selenide layers and quantum wells discussed in this work should allow us to study also the other unusual phenomena in low-dimensional mercury–iron selenide as the behavior of scattering superlattices or doping quantum wells. The preparation of corresponding samples by MBE is in progress.

VI. SUMMARY

Quantum-well structures of the semimagnetic narrow-gap semiconductor HgSe:Fe have been grown by MBE on ZnTe/GaAs substrates. The optimization of the growth of the ZnTe buffer layers has been performed using a method for the *in situ* determination of mosaic-structure parameters by RHEED. The critical thickness of HgSe:Fe on ZnTe has been analyzed as well by x-ray diffraction measurements as by time-dependent intensity-profile analysis of the RHEED pattern. It has been found that a growth-mode transition from a two-dimensional layer-by-layer growth to a three-dimensional Stranski-Krastanov growth mode occurs near the theoretical equilibrium value predicted by the Matthews-Blakeslee model. Due to the extended stability of this transition mode, the onset of the plastic relaxation in the HgS:Fe layer is delayed up to a layer thickness of 280 nm. This can be attributed, besides others, to the very low growth temperatures in the MBE of mercury–iron selenide. Magnetotransport investigations have been carried out on different HgSe:Fe quantum-well structures, corroborating the existence of a two-dimensional electron system (Q2D) for quantum-well dimensions of less than 20 nm. By variation of the quantum-well size, the subband splitting in HgSe:Fe has been investigated. From investigations of the quantum-Hall-plateau broadening, a damping parameter Γ of at least 6 meV has been determined experimentally. This value should allow us to distinguish in further experiments the contributions of the internal and the external localization to the plateau structure of the Hall voltage and, therefore, to study, in future work, the predicted[3] gradual transition from the Q2D quantum-Hall effect to the three-dimensional analog of the QHE.

ACKNOWLEDGMENTS

We thank Cornelia Prott and Ulrich Niggemeier for the support during the growth experiments. The work has been supported by Deutsche Forschungsgemeinschaft.

[1]For a comprehensive review of the physical properties of HgSe and HgSe:Fe bulk crystals, see R. R. Galazka and J. Kossut, in *Narrow Gap Semiconductors, Physics and Applications,* edited by W. Zawadzki, Lecture Notes in Physics Vol. 133 (Springer-Verlag, New York, 1980), p. 245 and references therein.

[2]J. Kossut, Z. Wilamowski, T. Dietl, and K. Swiatek, Solid State Commun. **73**, 883 (1990).

[3]M. von Ortenberg, Adv. Solid State Phys. **31**, 261 (1991).

[4]Y. Lansari, J. Ren, B. Sneed, K. A. Bowers, J. W. Cook, Jr., and J. F. Schetzina, Appl. Phys. Lett. **61**, 2554 (1992).

[5]G. Machel and M. von Ortenberg (unpublished).

[6]S. Tatarenko, J. Cibert, K. Saminadayar, P. H. Jouneau, V. H. Etgens, M. Sauvage-Simkin, and R. Pinchaux, J. Cryst. Growth **127**, 339 (1993).

[7]S. Bauer, A. Rosenauer, P. Link, W. Kuhn, J. Zweck, and W. Gebhardt, Ultramicroscopy **51**, 221 (1993).

[8]M. Lang, D. Schikora, Th. Widmer, C. Giftge, A. Forstner, V. Holy, J. Humenberger, K. Lischka, G. Brunthaler, H. Sitter, and M. von Ortenberg, J. Cryst. Growth **138**, 81 (1994).

[9]H. Ogawa, M. Nishio, M. Ikejiri, and H. Tuboi, Appl. Phys. Lett. **58**, 2384 (1991).

[10]M. Lang, Ph.D. thesis, University of Linz, Austria, 1993.

[11]K. Giftge, Ph.D. thesis, Technical University of Braunschweig, Germany, 1995.

[12]V. Holy, J. Kubena, E. Abramof, K. Lischka, A. Pesek, and E. Koppensteiner, J. Appl. Phys. **74**, 3 1736 (1993).

[13]E. F. Schubert, J. M. Kuo, R. F. Kopf, A. S. Jordan, H. S. Luftman, and J. C. Hopkins, Phys. Rev. B **42**, 1364 (1990).

[14]Z. Willamowski, A. Mycielski, W. Jantsch, and G. Hendorfer,

in *Proceedings of the 19th ICPS,* edited by W. Zawadzki (Polish Academy of Science, Warsaw, 1988), p. 1225.
[15]W. Dobrowolski, K. Dybko, A. Mycielski, J. Wtobel, S. Piechota, M. Palczewska, H. Szymczak, and Z. Willamowski, in *Proceedings of the 18th ICPS,* edited by O. Engstrom (World Scientific, Singapore, 1986), p. 1743.
[16]F. Pool, J. Kossut, U. Debska, and R. Reifenberger, Phys. Rev. B **35**, 3900 (1987).
[17]Th. Widmer, D. Schikora, C. Prott, B. Schoettker, M. v. Ortenberg, and K. Lischka (unpublished).
[18]F. C. Frank and J. H. van der Merwe, Proc. R. Soc. London Ser. A **198**, 205 (1949).
[19]J. W. Matthewsd and A. E. Blakeslee, J. Cryst. Growth **27**, 118 (1974).
[20]B. Dodson and J. Y. Tsao, Appl. Phys. Lett. **51**, 1325 (1987).
[21]I. J. Fritz, Appl. Phys. Lett. **51**, 1080 (1987).
[22]C. W. Snyder, B. G. Orr, D. Kessler, and L. M. Sander, Phys. Rev. Lett. **66**, 23 3032 (1991).
[23]P. R. Berger, K. Chang, P. Bhattacharya, and J. Singh, Appl. Phys. Lett. **53**, 684 (1988).
[24]M. Gendry, V. Drout, C. Santinelli, and G. Hollinger, Appl. Phys. Lett. **60**, 2249 (1992).
[25]D. J. Eaglesham and M. Cerullo, Phys. Rev. Lett. **64**, 1943 (1990).
[26]P. M. J. Maree, K. Nakagawa. F. Mulders, and J. F. van der Veen, Surf. Sci. **191**, 305 (1987).
[27]G. Springholz and G. Bauer, Phys. Rev. B **48**, 10 998 (1993).
[28]D. J. Srolovitz, Acta Metall. **37**, 621 (1989).
[29]G. Nachtwei, J. N. Bassom, R. J. Nicholas, U. Preppernau, and R. Herrmann, Semicond. Sci. Technol. **4**, 747 (1988).
[30]M. von Ortenberg, O. Portugal, W. Dobrowolski, A. Mycielski, R. Galazka, and F. Herlach, J. Phys. C **21**, 5393 (1988).
[31]W. Jantsch and Z. Wilamowski, in *Localization and Confinement of Electrons in Semiconductors,* edited by F. Kuchar, H. Heinrich, and G. Bauer, Springer Series in Solid State Sciences Vol. 97 (Springer-Verlag, Berlin, 1990), p. 137.
[32]Z. Wilamowski, K. Swiatek, T. Dietl, and J. Kossut, Solid State Commun. **74**, 8 (1990); **74**, 833 (1990).
[33]C. R. Pidgeon and R. N. Brown, Phys. Rev. **146**, 575 (1966).

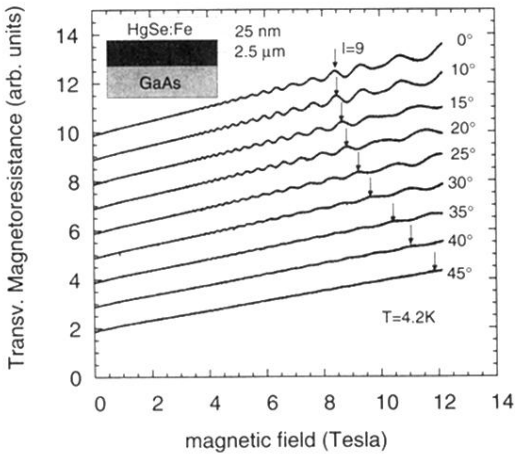

FIG. 4. Transversal magnetoresistance of a 25-nm HgSe:Fe single-quantum-well grown on ZnTe. The ninth Landau-level $I=9$ (marked by arrows) shifts in tilted magnetic fields.

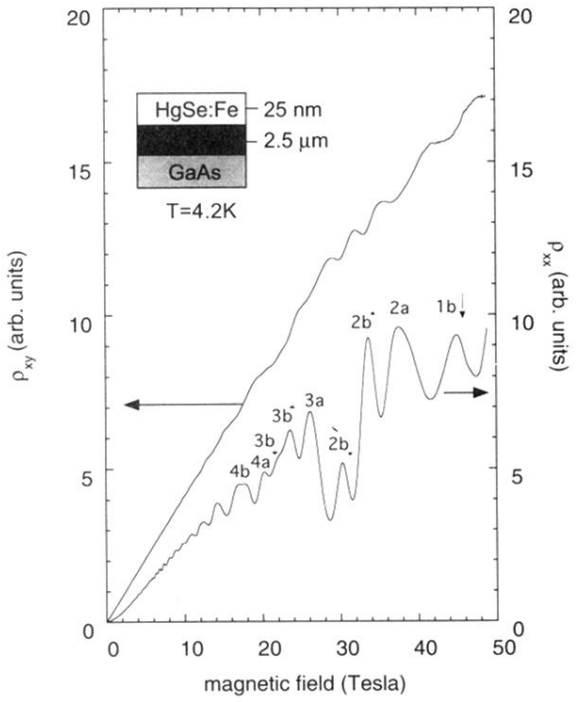

FIG. 6. Hall resistance and transversal magnetoresistance versus magnetic field of a 25-nm HgSe:Fe SQW. At least two different subbands are resolvable. The maximum values in the transversal magnetoresistance, which could be attributed to different subbands in the quantum well, are denoted by *a* and *b*. The assignment of the SdH maxima to the Landau levels have been performed using a simulation of the Landau-level splitting, which is described in Ref. 33.

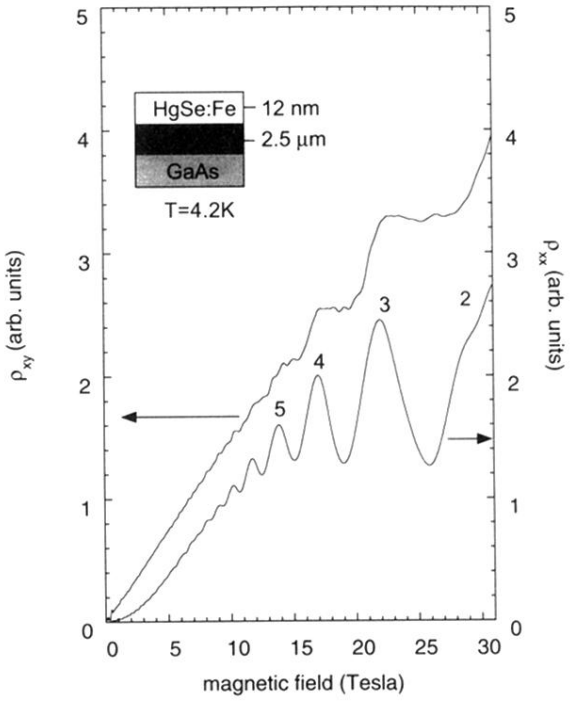

FIG. 7. Hall resistance and transversal magnetoresistance versus magnetic field for a 12-nm HgSe:Fe SQW. The Landau quantum number l is indicated and makes clear that the system is near the quantum limit. The data exhibit clearly one Q2D Landau ladder without spin splitting of a highly degenerated carrier system corresponding to bulk concentration $n = 3.8 \times 10^{18}\ \mathrm{cm}^{-3}$.